

Quantum analysis of polarization entanglement degradation induced by multiple-photon-pair generation

Richard A. Brewster^{1,*}, Gerald Baumgartner,² and Yanne K. Chembo¹

¹*University of Maryland, Department of Electrical and Computer Engineering and Institute for Research in Electronics and Applied Physics (IREAP), 8279 Paint Branch Drive, College Park, Maryland 20742, USA*

²*Laboratory for Telecommunication Sciences, 8080 Greenmead Drive, College Park, Maryland 20740, USA*



(Received 1 May 2021; accepted 15 July 2021; published 11 August 2021)

Polarization-encoded entanglement remains the simplest platform for the generation, manipulation, and visualization of entangled-photon states. While quantum dots have the potential to emit on-demand polarization entanglement, spontaneous-parametric-down-conversion (SPDC) sources remain the leading method for the generation of polarization-entangled states. SPDC sources suffer from the potential to produce multiple photon pairs in a single pass of an experiment. These multiple pairs have been shown to have negative impacts on quantum experiments involving entanglement. In this work, we now provide a rigorous theoretical model for the loss of entanglement due to additional photon pairs. This is seen as a reduction in a possible measurement of the Clauser-Horne-Shimony-Holt (CHSH) parameter. We perform these calculations for two different methods for the generation of polarization entanglement involving SPDC. The results agree with other observations presented in the literature. We also find that, even for small mean photon numbers, the CHSH parameter is reduced linearly, demonstrating that multiple photon pairs have a critical impact on the entanglement in the system.

DOI: [10.1103/PhysRevA.104.022411](https://doi.org/10.1103/PhysRevA.104.022411)

I. INTRODUCTION

The field of quantum communications offers various improvements over classical network communications, such as the potential for novel telecommunication protocols [1] and the generation of shared security keys [2]. Many of the protocols of quantum communications require the generation and distribution of entangled states throughout a quantum network. Entanglement can be encoded in a variety of photon-based carriers, such as energy-time [3–5], orbital angular momentum [6], and, more recently time-frequency bins [7–9]. While polarization-based entanglement distribution has technical issues when supporting long-distance quantum communication, it remains the simplest implementation method with respect to local entanglement generation and operations.

Polarization entanglement has been long studied and characterized [10–26]. A majority of these studies have relied on polarization entanglement generated using the spontaneous-parametric-down-conversion (SPDC) process [10–21]. Ideally, only a single photon pair should be produced to construct an entangled state that is robust against entanglement degradation. However, it is well known that SPDC has the potential to generate multiple photon pairs. While polarization entanglement generated from quantum dot sources have the potential to produce on-demand single-photon polarization-entangled states [26], using SPDC sources is still a simpler method for the generation of entangled states. Therefore, we will develop a rigorous theoretical model that shows the reduction in en-

tanglement quality due to the generation of multiple pairs by an SPDC source.

We characterize the quality of entanglement using measured values of the Clauser-Horne-Shimony-Holt (CHSH) parameter S [27]. The CHSH inequality dictates that if $|S| > 2$ then no local classical theory could have predicted the coincidences [27]. The maximum value of S permitted by quantum mechanics is $|S| = 2\sqrt{2}$ [28].

Several previous studies have analyzed the effects of multiple photon pairs [19,29–32] on the value of S . It is well known that the multiple photon pairs often generated by SPDC contribute accidental coincidences to two-photon interference experiments [30,31]. Since the CHSH experiment relies on two-photon coincidence measurements, it is similarly impacted. However, these studies have capped the maximum number of photon pairs [29] or made use of classical probability distributions [19,30–32] to describe the number of photon pairs generated. The classical distribution approach works for most experiments, but it would be difficult to use this approach to compute the result after additional quantum evolutions. We will develop an all-quantum theory from first principles.

There are two main methods to generate a maximally entangled Bell state using SPDC in fiber-based systems. These methods are outlined in Fig. 1. In Fig. 1(a), a 50:50 beam splitter is used to convert a correlated photon pair generated by an SPDC source into an entangled Bell state [15,16]. In Fig. 1(b), the placement of an SPDC source inside of a Sagnac-like interferometer produces an entangled state [17–21]. Recently, this method has been used more frequently because it has been shown to be more efficient [17]. In this paper, we study the effects that the multiple pairs emitted by the SPDC source

*Corresponding author: ykchembo@umd.edu

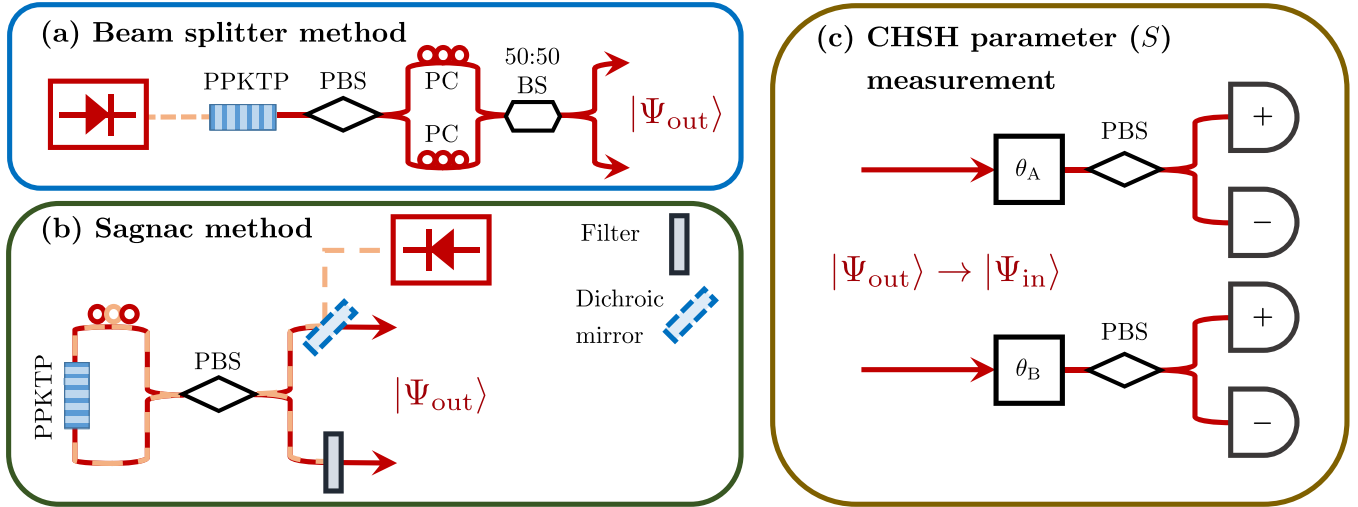


FIG. 1. Two different methods for generating a $|\Psi^-\rangle$ Bell state using type-II spontaneous parametric down conversion (SPDC). (a) The beam-splitter method. A pumped periodically poled potassium-titanyl-phosphate (PPKTP) crystal generates orthogonally polarized photon pairs. These pairs are split using a polarizing beam splitter (PBS) and then subsequently inserted into a 50:50 beam splitter (BS). This generates the $|\Psi^-\rangle$ Bell state along with two additional terms that do not contribute to the coincidence counts. As such, this is not the most efficient method for the generation of an entangled state. (b) The Sagnac method. The pump is set to be diagonally polarized. The pump photons are reflected by a dichroic mirror and subsequently split at a horizontal-vertical PBS. The clockwise and counterclockwise propagating pulses in the Sagnac interferometer will generate the two terms of the Bell state. Since both of these setups rely on SPDC, there exists a probability of multiple-pair generation. This could affect the quality of the resulting entanglement. The exact state emitted is labeled as $|\Psi_{\text{out}}\rangle$ in both setups. The polarization controllers (PC) shown in both methods maintain the polarization state of the photons, but we will neglect them in the main text. (c) Method for performing a Clauser-Horne-Shimony-Holt (CHSH) inequality measurement. The polarization-encoded entangled state $|\Psi^-\rangle$, which is simultaneously propagating along two separate spatial paths, is input into two polarization controllers. These devices rotate the polarization vector by the angle θ_A in one path and the angle θ_B in the other path. Following these rotations, the photons in both paths enter ideal polarization beam splitters (PBS) that send horizontally polarized photons toward the “+” detectors and vertically polarized photons toward the “-” detectors. Coincidences measured between various combinations of these four detectors are recorded and used to compute the CHSH parameter, S , as discussed in the main text.

have in both of these systems, in terms of the CHSH parameter S as measured in Fig. 1(c).

Ideally, both of these approaches would produce the two-photon maximally entangled Bell state $|\Psi^-\rangle$ defined as

$$|\Psi^-\rangle \equiv \frac{1}{\sqrt{2}}(\hat{a}_H^\dagger \hat{b}_V^\dagger - \hat{a}_V^\dagger \hat{b}_H^\dagger)|0\rangle, \quad (1)$$

where \hat{a}^\dagger is the creation operator for spatial path A, \hat{b}^\dagger is the creation operator for spatial path B, and $|0\rangle$ is the vacuum state. The subscript “H” represents a horizontally polarized photon in Eq. (1), and the subscript “V” represents a vertically polarized photon. However, this state would only occur when a single pair of orthogonally polarized photons was emitted by the pumped periodically poled potassium-titanyl-phosphate (PPKTP) crystals of Fig. 1. Because these crystals emit photon pairs through the type-II SPDC process, the output state generated by the SPDC sources is more complicated than the simple Bell state shown in Eq. (1). The main contribution of this paper will be performing the calculation of the CHSH parameter for both configurations and evaluating the degradation of entanglement that results from the generation of incidental multiple pairs by the source. This will be done using a fully quantum theoretical approach based on the Husimi-Kano Q function.

This work is outlined as follows. In Sec. II, we develop the theoretical model for the degradation of the CHSH parameter

measured due to multiple pairs for the entangled states generated by the setup of Fig. 1(a) [beam-splitter method], while in Sec. III we focus on the Fig. 1(b) [Sagnac method]. Remarks and conclusions are given in the last section of the article.

II. BEAM-SPLITTER METHOD

A. Formal definition of the CHSH parameter

We will start with the simpler beam-splitter method of Fig. 1(a). As mentioned above, the pumped PPKTP crystal produces pairs of orthogonally polarized photons through the SPDC process. The full quantum Hamiltonian that describes this interaction is given by [33]

$$\hat{H} = i\kappa(\hat{c}^\dagger \hat{a}_H \hat{a}_V - \hat{c} \hat{a}_H^\dagger \hat{a}_V^\dagger), \quad (2)$$

where κ is a coupling constant and \hat{c}^\dagger is the creation operator for photons in the pump beam. We now make the usual classical pump approximation [33]. For a strong coherent pump with coherent state parameter γ_0 , we set $\hat{c} \rightarrow \langle \hat{c} \rangle = \gamma_0$ and $\hat{c}^\dagger \rightarrow \langle \hat{c}^\dagger \rangle = \gamma_0^*$ in Eq. (2), giving

$$\hat{H} = i\kappa(\gamma_0^* \hat{a}_H \hat{a}_V - \gamma_0 \hat{a}_H^\dagger \hat{a}_V^\dagger). \quad (3)$$

This Hamiltonian corresponds to the unitary evolution operator with interaction time τ given as

$$\hat{U} \equiv e^{-i\hat{H}\tau} = e^{s(\hat{a}_H \hat{a}_V - \hat{a}_H^\dagger \hat{a}_V^\dagger)}, \quad (4)$$

where we have let γ_0 be real and defined the two-mode squeezing parameter as $s = \gamma_0 \kappa \tau$. It can be shown [34,35] that the unitary evolution operator of Eq. (4) can be factored as

$$\hat{U} = \frac{e^{-\tanh(s)\hat{a}_H^\dagger\hat{a}_V^\dagger}}{\cosh(s)} \left[\frac{1}{\cosh(s)} \right]^{\hat{a}_H^\dagger\hat{a}_H + \hat{a}_V^\dagger\hat{a}_V} e^{\tanh(s)\hat{a}_H\hat{a}_V}. \quad (5)$$

Neglecting the pump beam, the state following the PPKTP crystal is now given by the application of the unitary evolution operator acting on the vacuum state $|0\rangle$. Thus, we have that

$$\begin{aligned} |\psi\rangle &= \hat{U}|0\rangle \\ &= \frac{e^{-\tanh(s)\hat{a}_H^\dagger\hat{a}_V^\dagger}}{\cosh(s)} \left[\frac{1}{\cosh(s)} \right]^{\hat{a}_H^\dagger\hat{a}_H + \hat{a}_V^\dagger\hat{a}_V} e^{\tanh(s)\hat{a}_H\hat{a}_V} |0\rangle \\ &= \frac{e^{-\tanh(s)\hat{a}_H^\dagger\hat{a}_V^\dagger}}{\cosh(s)} |0\rangle \\ &= \frac{1}{\cosh(s)} \sum_{j=0}^{\infty} \frac{1}{j!} [-\tanh(s)]^j \hat{a}_H^{\dagger j} \hat{a}_V^{\dagger j} |0\rangle, \end{aligned} \quad (6)$$

which is known as the two-mode squeezed vacuum state [33]. Inspection of Eq. (6) reveals that the pumped PPKTP crystal has the potential to generate any number of photon pairs.

After the ideal polarizing beam splitter (PBS), the state in Eq. (6) becomes

$$|\psi\rangle \rightarrow \frac{e^{-\tanh(s)\hat{a}_H^\dagger\hat{b}_V^\dagger}}{\cosh(s)} |0\rangle, \quad (7)$$

where we have made the transformation $\hat{a}_V^\dagger \rightarrow \hat{b}_V^\dagger$, which is a result of the vertically polarized photons being directed into path B while the horizontally polarized photons remain in path A. Paths A and B are recombined at the 50:50 beam splitter of Fig. 1(a). The beam splitter applies the following transformation to the operators,

$$\hat{a}_X^\dagger \rightarrow \frac{1}{\sqrt{2}}(\hat{a}_X^\dagger + i\hat{b}_X^\dagger), \quad \hat{b}_X^\dagger \rightarrow \frac{1}{\sqrt{2}}(\hat{b}_X^\dagger + i\hat{a}_X^\dagger), \quad (8)$$

where X denotes an arbitrary polarization state. Applying the transformation of Eq. (8) to the state of Eq. (7) gives the state after the 50:50 beam splitter, $|\Psi_{\text{out}}\rangle$, as

$$|\Psi_{\text{out}}\rangle = \frac{e^{-\tanh(s)(\hat{a}_H^\dagger\hat{b}_V^\dagger - \hat{a}_V^\dagger\hat{b}_H^\dagger + i\hat{a}_H^\dagger\hat{a}_V^\dagger + i\hat{b}_H^\dagger\hat{b}_V^\dagger)/2}}{\cosh(s)} |0\rangle. \quad (9)$$

Inspection of Eq. (7) reveals that it shares no resemblance to the ideal state of Eq. (1). To obtain the ideal state, we only want a single photon pair to be emitted by the pumped PPKTP crystal. This can be achieved by letting $s \approx 0$, so that we may truncate the $j > 1$ terms of Eq. (6). This gives the approximate state as

$$|\psi\rangle \approx \frac{1}{\cosh(s)} (1 - \tanh(s)\hat{a}_H^\dagger\hat{a}_V^\dagger) |0\rangle. \quad (10)$$

Applying the transformation due to the ideal PBS and 50:50 beam splitter now gives the output state as

$$\begin{aligned} |\Psi_{\text{out}}\rangle &\approx \frac{1}{\cosh(s)} \left[1 - \frac{\tanh(s)}{2} (\hat{a}_H^\dagger\hat{b}_V^\dagger - \hat{a}_V^\dagger\hat{b}_H^\dagger \right. \\ &\quad \left. + i\hat{a}_H^\dagger\hat{a}_V^\dagger + i\hat{b}_H^\dagger\hat{b}_V^\dagger) \right] |0\rangle. \end{aligned} \quad (11)$$

Equation (11) is not exactly equal to the ideal Bell state of Eq. (1). However, the vacuum state term and the terms where two photons enter the same spatial path will not contribute coincidence counts in the measurement of the CHSH parameter depicted in Fig. 1(c). Neglecting these terms in Eq. (11) and renormalizing gives Eq. (1). It is important to note that the additional pairs in the full state of Eq. (9) will yield additional terms that will also contribute coincidence counts, and therefore cannot be neglected unless photon number resolving detectors are used to eliminate these multipair correlation events in postprocessing. These additional coincidence counts will negatively impact CHSH inequality experiments by reducing the value of the parameter S .

We now consider a measurement of the CHSH parameter for entangled states generated using the beam-splitter method. The output state $|\Psi_{\text{out}}\rangle$ of Eq. (9) now becomes the input state $|\Psi_{\text{in}}\rangle$ to the CHSH measurement system of Fig. 1(c). The polarization rotations in paths A and B transform the creation operators to

$$\begin{aligned} \hat{a}_H^\dagger &\rightarrow \cos\theta_A\hat{a}_H^\dagger + \sin\theta_A\hat{a}_V^\dagger, \\ \hat{a}_V^\dagger &\rightarrow \cos\theta_A\hat{a}_V^\dagger - \sin\theta_A\hat{a}_H^\dagger, \\ \hat{b}_H^\dagger &\rightarrow \cos\theta_B\hat{b}_H^\dagger + \sin\theta_B\hat{b}_V^\dagger, \\ \hat{b}_V^\dagger &\rightarrow \cos\theta_B\hat{b}_V^\dagger - \sin\theta_B\hat{b}_H^\dagger. \end{aligned} \quad (12)$$

Applying the transformations of Eq. (12) to the state in Eq. (9) gives the state after the polarization rotations $|\psi\rangle$ as

$$\begin{aligned} |\psi\rangle &= \frac{1}{\cosh(s)} e^{-\tanh(s)\cos(\theta_A - \theta_B)(\hat{a}_H^\dagger\hat{b}_V^\dagger - \hat{a}_V^\dagger\hat{b}_H^\dagger)/2} \\ &\quad \times e^{-\tanh(s)\sin(\theta_A - \theta_B)(\hat{a}_H^\dagger\hat{b}_H^\dagger + \hat{a}_V^\dagger\hat{b}_V^\dagger)/2} \\ &\quad \times e^{i\tanh(s)\sin(2\theta_A)(\hat{a}_H^{\dagger 2} - \hat{a}_V^{\dagger 2})/4} \\ &\quad \times e^{i\tanh(s)\sin(2\theta_B)(\hat{b}_H^{\dagger 2} - \hat{b}_V^{\dagger 2})/4} \\ &\quad \times e^{-i\tanh(s)[\cos(2\theta_A)\hat{a}_H^\dagger\hat{a}_V^\dagger + \cos(2\theta_B)\hat{b}_H^\dagger\hat{b}_V^\dagger]/2} |0\rangle. \end{aligned} \quad (13)$$

Before we define the CHSH parameter, we first define the correlation coefficient $E(\theta_A, \theta_B)$ as [27]

$$E(\theta_A, \theta_B) = \frac{R_{++} + R_{--} - R_{+-} - R_{-+}}{R_{++} + R_{--} + R_{+-} + R_{-+}}, \quad (14)$$

where the $R_{\pm\mp}$ is the measurable coincidence rate between the \pm detector in path A and the \mp detector in path B. For number insensitive detectors, the coincidence rates are computed, theoretically, as

$$\begin{aligned} R_{++} &\propto \langle \hat{a}_H^\dagger\hat{a}_H\hat{b}_H^\dagger\hat{b}_H \rangle, \quad R_{--} \propto \langle \hat{a}_V^\dagger\hat{a}_V\hat{b}_V^\dagger\hat{b}_V \rangle, \\ R_{+-} &\propto \langle \hat{a}_H^\dagger\hat{a}_H\hat{b}_H^\dagger\hat{b}_V \rangle, \quad R_{-+} \propto \langle \hat{a}_V^\dagger\hat{a}_V\hat{b}_H^\dagger\hat{b}_H \rangle, \end{aligned} \quad (15)$$

where we have used the convention that the ideal PBS of Fig. 1(c) directs horizontally polarized photons to the “+” detectors and vertically polarized photons to the “−” detectors. With the correlation of Eq. (14), we may now compute the CHSH parameter as [27]

$$S \equiv E\left(0, \frac{\pi}{8}\right) - E\left(0, \frac{3\pi}{8}\right) + E\left(\frac{\pi}{4}, \frac{\pi}{8}\right) + E\left(\frac{\pi}{4}, \frac{3\pi}{8}\right). \quad (16)$$

Inspection of Eq. (13) reveals that it will be difficult to use the state after the rotation of the polarization vectors to compute the rates of Eq. (15), since this would require the computation of intractable series summations. To simplify this calculation, we now switch to using the Husimi-Kano Q function [36–38], as developed in the next subsection.

B. Calculating coincidence rates using the Husimi-Kano function

To calculate the expectation values in Eq. (15), we use the fact that the expectation value of an arbitrary combination of creation and annihilation operators, \hat{A} , can be obtained by integrating the classical representation of the antinormally ordered operators with the Q function [38]

$$\langle \hat{A} \rangle = \int d^2\alpha \mathcal{A}^{(a)}(\alpha) Q(\alpha), \quad (17)$$

where $\mathcal{A}^{(a)}$ is the classical (complex-valued) representation of the antinormally ordered operator \hat{A} with $\hat{a} \rightarrow \alpha$ and $\hat{a}^\dagger \rightarrow \alpha^*$. The Q function is a quasiprobability distribution that is typically defined as [38]

$$Q(\alpha) \equiv \frac{1}{\pi} \langle \alpha | \hat{\rho} | \alpha \rangle, \quad (18)$$

where $\hat{\rho}$ is the density operator for the state and $|\alpha\rangle$ is a sample coherent state with state parameter α . This coherent state parameter acts as the complex independent variable of the distribution.

The Q function as defined in Eq. (18) is only capable of describing a single photonic mode. However, there are four photonic modes represented in the state of Eq. (13). Therefore, we generalize the Q function of Eq. (18) as

$$Q(\alpha_H, \alpha_V, \beta_H, \beta_V) \equiv \frac{1}{\pi^4} \langle \beta_V | \langle \beta_H | \langle \alpha_V | \langle \alpha_H | \hat{\rho} | \alpha_H \rangle | \alpha_V \rangle | \beta_H \rangle | \beta_V \rangle, \quad (19)$$

where the coherent state parameters $\alpha_H, \alpha_V, \beta_H,$ and β_V are the independent variables used to describe the modes represented by the creation operators $\hat{a}_H^\dagger, \hat{a}_V^\dagger, \hat{b}_H^\dagger,$ and $\hat{b}_V^\dagger,$ respectively. Note that Eq. (19) is now a four-mode Q function.

The Q function is typically used when one has macroscopic states that contain many photons, but the Q function can be used to express single-photon states as well. Ideally, the SPDC source of Fig. 1(a) would only emit a single pair of photons; however, we wish to also consider the case when multiple photon pairs are emitted. This is why we choose to use the Q function representation. The Q function allows us to write the general state emitted from the SPDC source in closed form. This representation also has the advantage of being indifferent to whether the state is close to being a single photon or is macroscopic.

Using the pure state of Eq. (13) in Eq. (19) gives the Q function for the state after the polarization rotation of Fig. 1(c) as

$$Q(\alpha_H, \alpha_V, \beta_H, \beta_V) = \frac{1}{\pi^4 \cosh^2(s)} e^{-(|\alpha_H|^2 + |\alpha_V|^2 + |\beta_H|^2 + |\beta_V|^2)}$$

$$\begin{aligned} & \times e^{-\tanh(s) \cos(\theta_A - \theta_B) (\alpha_H \beta_V + \alpha_H^* \beta_V^* - \alpha_V \beta_H - \alpha_V^* \beta_H^*)/2} \\ & \times e^{-\tanh(s) \sin(\theta_A - \theta_B) (\alpha_H \beta_H + \alpha_H^* \beta_H^* + \alpha_V \beta_V + \alpha_V^* \beta_V^*)/2} \\ & \times e^{i \tanh(s) \sin(2\theta_A) (\alpha_H^2 - \alpha_H^{*2} - \alpha_V^2 + \alpha_V^{*2})/4} \\ & \times e^{i \tanh(s) \sin(2\theta_B) (\beta_H^2 - \beta_H^{*2} - \beta_V^2 + \beta_V^{*2})/4} \\ & \times e^{-i \tanh(s) \cos(2\theta_A) (\alpha_H \alpha_V - \alpha_H^* \alpha_V^*)/2} \\ & \times e^{-i \tanh(s) \cos(2\theta_B) (\beta_H \beta_V - \beta_H^* \beta_V^*)/2}. \end{aligned} \quad (20)$$

It is important to note that the four-mode Q function relies on four complex variables, thus requiring eight real independent variables. To use the Q function of Eq. (20) to compute the rates of Eq. (15), we will need to compute eight-dimensional integrals. In order to compute expectation values using the Q function, we must first express observables in antinormal order [38]. Antinormal order requires all annihilation operators to be on the left of each term and all creation operators to be on the right. If we focus on the rate R_{++} , the required observable expressed in antinormal order is given simply as

$$\begin{aligned} \hat{a}_H^\dagger \hat{a}_H \hat{b}_H^\dagger \hat{b}_H &= (\hat{a}_H \hat{a}_H^\dagger - 1)(\hat{b}_H \hat{b}_H^\dagger - 1) \\ &= \hat{a}_H \hat{a}_H^\dagger \hat{b}_H \hat{b}_H^\dagger - \hat{a}_H \hat{a}_H^\dagger - \hat{b}_H \hat{b}_H^\dagger + 1, \end{aligned} \quad (21)$$

where we have used the commutation relation for the creation and annihilation operators. We next replace $\hat{a}_H \rightarrow \alpha_H, \hat{a}_H^\dagger \rightarrow \alpha_H^*, \hat{b}_H \rightarrow \beta_H,$ and $\hat{b}_H^\dagger \rightarrow \beta_H^*$, before inserting the resulting expression in an integral over the Q function [38]. Performing this procedure for Eq. (21) and the other observables of Eq. (15) gives the rates using the Q function as

$$\begin{aligned} R_{++} &= \int d^2\alpha_H d^2\alpha_V d^2\beta_H d^2\beta_V Q(\alpha_H, \alpha_V, \beta_H, \beta_V) \\ & \quad \times (|\alpha_H|^2 |\beta_H|^2 - |\alpha_H|^2 - |\beta_H|^2 + 1), \\ R_{--} &= \int d^2\alpha_H d^2\alpha_V d^2\beta_H d^2\beta_V Q(\alpha_H, \alpha_V, \beta_H, \beta_V) \\ & \quad \times (|\alpha_V|^2 |\beta_V|^2 - |\alpha_V|^2 - |\beta_V|^2 + 1), \\ R_{+-} &= \int d^2\alpha_H d^2\alpha_V d^2\beta_H d^2\beta_V Q(\alpha_H, \alpha_V, \beta_H, \beta_V) \\ & \quad \times (|\alpha_H|^2 |\beta_V|^2 - |\alpha_H|^2 - |\beta_V|^2 + 1), \\ R_{-+} &= \int d^2\alpha_H d^2\alpha_V d^2\beta_H d^2\beta_V Q(\alpha_H, \alpha_V, \beta_H, \beta_V) \\ & \quad \times (|\alpha_V|^2 |\beta_H|^2 - |\alpha_V|^2 - |\beta_H|^2 + 1), \end{aligned} \quad (22)$$

where $d^2\alpha_H$ is the differential over the real and imaginary parts of α_H and similarly for the other three variables. Using the Q function of Eq. (20) in Eq. (22) and performing the integrals is a multistep process which is detailed in the next subsection.

C. Computation of the coincidence rates integrals

Computing the coincidence rates of Eq. (15) involves evaluating the eight-dimensional integrals of Eq. (22) over the real and imaginary parts of the four complex variables in the Q function defined by Eq. (19). Ordinarily, these integrals would be very difficult to compute directly. However, we may

use the fact that the Q functions for the output states of the beam-splitter method and the Sagnac method are represented by multidimensional Gaussian normal distributions. This fact significantly reduces the analytic complexity of the integrals.

A general multidimensional normal distribution may be represented as

$$P(\mathbf{x}) = \frac{1}{\sqrt{(2\pi)^N \text{Det}(\boldsymbol{\Sigma})}} e^{-(\mathbf{x}-\boldsymbol{\mu}) \cdot [\boldsymbol{\Sigma}^{-1}(\mathbf{x}-\boldsymbol{\mu})]/2}, \quad (23)$$

where N is the number of dimensions, \mathbf{x} is a vector of the sampling variables of the distribution, $\boldsymbol{\mu}$ is a vector of the means of the sampling variables, and $\boldsymbol{\Sigma}$ is the covariance matrix. The elements of the covariance matrix can be defined using the central second moments of the distribution $P(\mathbf{x})$, giving

$$\Sigma_{jk} \equiv \int d^N x (x_j - \mu_j)(x_k - \mu_k) P(\mathbf{x}), \quad (24)$$

where $d^N x$ is the product of the differentials over each of the N independent variables, and the integration is over all space.

Note that the coincidence rate definitions of Eq. (22) are equivalent to taking higher moments of the Q function. If we let the sampling vector \mathbf{x} be an eight-dimensional vector defined using the complex variables of the Q function of Eq. (19) as

$$\begin{aligned} x_1 + ix_2 &\equiv \alpha_H, & x_3 + ix_4 &\equiv \alpha_V, \\ x_5 + ix_6 &\equiv \beta_H, & x_7 + ix_8 &\equiv \beta_V, \end{aligned} \quad (25)$$

then the rate R_{++} of Eq. (22) can be written as

$$\begin{aligned} R_{++} = \int d^8 x (x_1^2 x_5^2 + x_1^2 x_6^2 + x_2^2 x_5^2 + x_2^2 x_6^2 \\ - x_1^2 - x_2^2 - x_5^2 - x_6^2 + 1) P(\mathbf{x}), \end{aligned} \quad (26)$$

where we have let $N = 8$, and the distribution $P(\mathbf{x})$ of Eq. (23) is replaced with a Gaussian normal Q function. The higher moments of a normal distribution can be computed using the second moments. It can be shown that, for general N ,

$$\int d^N x x_j^2 x_k^2 P(\mathbf{x}) = \Sigma_{jj} \Sigma_{kk} + 2 \Sigma_{jk}^2, \quad (27)$$

where we have used the fact that $\Sigma_{jk} = \Sigma_{kj}$. Using Eqs. (24), (27), and the fact that $P(\mathbf{x})$ is normalized gives the integral of Eq. (26) as

$$\begin{aligned} R_{++} = \Sigma_{11} \Sigma_{55} + \Sigma_{11} \Sigma_{66} + \Sigma_{22} \Sigma_{55} + \Sigma_{22} \Sigma_{66} \\ + 2 \Sigma_{15}^2 + 2 \Sigma_{16}^2 + 2 \Sigma_{25}^2 + 2 \Sigma_{26}^2 \\ - \Sigma_{11} - \Sigma_{22} - \Sigma_{55} - \Sigma_{66} + 1. \end{aligned} \quad (28)$$

We use this procedure for the other three coincidence rates, obtaining

$$\begin{aligned} R_{--} = \Sigma_{33} \Sigma_{77} + \Sigma_{33} \Sigma_{88} + \Sigma_{44} \Sigma_{77} + \Sigma_{44} \Sigma_{88} \\ + 2 \Sigma_{37}^2 + 2 \Sigma_{38}^2 + 2 \Sigma_{47}^2 + 2 \Sigma_{48}^2 \\ - \Sigma_{33} - \Sigma_{44} - \Sigma_{77} - \Sigma_{88} + 1, \\ R_{+-} = \Sigma_{11} \Sigma_{77} + \Sigma_{11} \Sigma_{88} + \Sigma_{22} \Sigma_{77} + \Sigma_{22} \Sigma_{88} \\ + 2 \Sigma_{17}^2 + 2 \Sigma_{18}^2 + 2 \Sigma_{27}^2 + 2 \Sigma_{28}^2 \\ - \Sigma_{11} - \Sigma_{22} - \Sigma_{77} - \Sigma_{88} + 1, \end{aligned}$$

$$\begin{aligned} R_{-+} = \Sigma_{33} \Sigma_{55} + \Sigma_{33} \Sigma_{66} + \Sigma_{44} \Sigma_{55} + \Sigma_{44} \Sigma_{66} \\ + 2 \Sigma_{35}^2 + 2 \Sigma_{36}^2 + 2 \Sigma_{45}^2 + 2 \Sigma_{46}^2 \\ - \Sigma_{33} - \Sigma_{44} - \Sigma_{55} - \Sigma_{66} + 1. \end{aligned} \quad (29)$$

Now, the Q function of Eq. (20) is a multidimensional Gaussian normal distribution with $N = 8$ and a mean of zero. Thus, the vector $\boldsymbol{\mu} = \mathbf{0}$ and inspection of Eq. (23) reveals that, if $\boldsymbol{\mu} = \mathbf{0}$, we may simply read off the values of $\boldsymbol{\Sigma}^{-1}$ from Eq. (20). We may then invert $\boldsymbol{\Sigma}^{-1}$ to compute the covariance matrix $\boldsymbol{\Sigma}$. Once the covariance matrix is obtained, we can compute the integrals using the expressions for the coincidence rates, such as the one in Eq. (28).

Following this procedure, we use the output Q function for the beam-splitter method, which is given by Eq. (20), to find that the elements of the matrix $\boldsymbol{\Sigma}^{-1}$ are

$$\begin{aligned} \Sigma_{11}^{-1} = \Sigma_{22}^{-1} = \Sigma_{33}^{-1} = \Sigma_{44}^{-1} \\ = \Sigma_{55}^{-1} = \Sigma_{66}^{-1} = \Sigma_{77}^{-1} = \Sigma_{88}^{-1} = 2, \\ \Sigma_{12}^{-1} = -\Sigma_{34}^{-1} = \sin(2\theta_A) \tanh(s), \\ \Sigma_{14}^{-1} = \Sigma_{23}^{-1} = -\cos(2\theta_A) \tanh(s), \\ \Sigma_{15}^{-1} = -\Sigma_{26}^{-1} = \Sigma_{37}^{-1} = -\Sigma_{48}^{-1} \\ = \sin(\theta_A - \theta_B) \tanh(s), \\ \Sigma_{17}^{-1} = -\Sigma_{28}^{-1} = -\Sigma_{35}^{-1} = \Sigma_{46}^{-1} \\ = \cos(\theta_A - \theta_B) \tanh(s), \\ \Sigma_{56}^{-1} = -\Sigma_{78}^{-1} = \sin(2\theta_B) \tanh(s), \\ \Sigma_{58}^{-1} = \Sigma_{67}^{-1} = -\cos(2\theta_B) \tanh(s), \end{aligned} \quad (30)$$

where we have used the fact that $\boldsymbol{\Sigma}^{-1}$ is a symmetric matrix; that is, $\Sigma_{jk}^{-1} = \Sigma_{kj}^{-1}$, and all of the elements not displayed in Eq. (30) are zero. We can invert $\boldsymbol{\Sigma}^{-1}$ using a symbolic processor such as MATHEMATICA, which gives the elements of the covariance matrix $\boldsymbol{\Sigma}$ as

$$\begin{aligned} \Sigma_{11} = \Sigma_{22} = \Sigma_{33} = \Sigma_{44} = \Sigma_{55} \\ = \Sigma_{66} = \Sigma_{77} = \Sigma_{88} = \frac{1}{8} [3 + \cosh(2s)], \\ -\Sigma_{12} = \Sigma_{34} = \frac{1}{8} \sin(2\theta_A) \sinh(2s), \\ \Sigma_{14} = \Sigma_{23} = \frac{1}{8} \cos(2\theta_A) \sinh(2s), \\ -\Sigma_{15} = \Sigma_{26} = -\Sigma_{37} = \Sigma_{48} \\ = \frac{1}{8} \sin(\theta_A - \theta_B) \sinh(2s), \\ -\Sigma_{17} = \Sigma_{28} = \Sigma_{35} = -\Sigma_{46} \\ = \frac{1}{8} \cos(\theta_A - \theta_B) \sinh(2s), \\ -\Sigma_{56} = \Sigma_{78} = \frac{1}{8} \sin(2\theta_B) \sinh(2s), \\ \Sigma_{58} = \Sigma_{67} = \frac{1}{8} \cos(2\theta_B) \sinh(2s), \\ -\Sigma_{16} = \Sigma_{25} = \Sigma_{38} = -\Sigma_{47} \\ = \frac{1}{4} \cos(\theta_A + \theta_B) \sinh^2(s), \\ -\Sigma_{18} = \Sigma_{27} = -\Sigma_{36} = \Sigma_{45} \\ = \frac{1}{4} \sin(\theta_A + \theta_B) \sinh^2(s), \end{aligned} \quad (31)$$

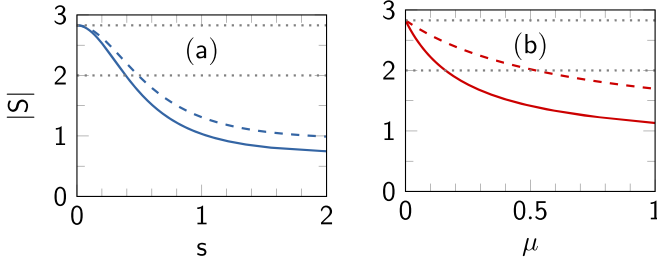


FIG. 2. Plots of the CHSH parameter $|S|$ for the state generated using the beam-splitter method of Fig. 1(a) given by Eq. (34) (solid lines) and the state generated using the Sagnac method of Fig. 1(b) given by Eq. (53) (dashed lines). The CHSH inequality is violated when $|S| > 2$ and is at its maximum when $|S| = 2\sqrt{2}$. These two values are indicated by the gray dotted lines. (a) Plots of $|S|$ as a function of the squeezing parameter s . (b) Plots of $|S|$ as a function of the mean photon number μ . All units are dimensionless. In all cases, we see that the state generated by the Sagnac method is more robust to the negative effects of multiple photon pairs than the state generated by the beam-splitter method.

where $\Sigma_{jk} = \Sigma_{kj}$ and the elements not listed are zero. Next, using the appropriate elements of Σ in Eqs. (28) and (29) gives the coincidence rates as

$$\begin{aligned} R_{++} = R_{--} &= \frac{1}{16} \{4 \sinh^4(s) [1 + \cos^2(\theta_A + \theta_B)] \\ &\quad + \sinh^2(2s) \sin^2(\theta_A - \theta_B)\}, \\ R_{+-} = R_{-+} &= \frac{1}{16} \{4 \sinh^4(s) [1 + \sin^2(\theta_A + \theta_B)] \\ &\quad + \sinh^2(2s) \cos^2(\theta_A - \theta_B)\}. \end{aligned} \quad (32)$$

With the coincidence rates of Eq. (32) in hand, we may now compute the correlation coefficient using Eq. (14) obtaining

$$\begin{aligned} E(\theta_A, \theta_B) &= -\frac{\cos(2\theta_A) \cos(2\theta_B) + \cosh(2s) \sin(2\theta_A) \sin(2\theta_B)}{2 \cosh(2s) - 1}. \end{aligned} \quad (33)$$

Finally, using Eq. (33) in Eq. (16) gives the magnitude of the CHSH parameter as

$$|S| = 2\sqrt{2} \frac{\cosh^2(s)}{2 \cosh(2s) - 1}. \quad (34)$$

The mean number of photon pairs μ for SPDC is given as $\mu = \sinh^2 s$ [33]. This allows us to represent the CHSH parameter using the mean photon pair generation rate as

$$|S| = 2\sqrt{2} \frac{1 + \mu}{1 + 4\mu}. \quad (35)$$

Equations (34) and (35) are remarkably simple expressions. They represent the reduction of the CHSH parameter due to the presence of additional photon pairs, and the corresponding plots are represented in Fig. 2(a). It is only when the mean photon number reaches zero that the CHSH parameter is at its maximum. Thus, for SPDC generated entangled states, there always exists some probability of an additional pair that degrades the CHSH parameter.

III. SAGNAC METHOD

A. Output quantum state

Having computed S for the experimental setup shown in Fig. 1(a), we now move to the more complicated Sagnac method setup shown in Fig. 1(b). The experimental setup for the Sagnac method requires more careful alignment than the beam-splitter setup. The analysis for the Sagnac method starts by examining the pump beam. The pump beam is aligned so that it is diagonally polarized before insertion into the PBS. For a strong coherent pump with coherent state parameter γ_0 , the state of the pump beam can then be written as

$$|\psi_{\text{pump}}\rangle = e^{-|\gamma_0|^2/2} e^{\gamma_0(\hat{c}_H^\dagger + \hat{c}_V^\dagger)/\sqrt{2}} |0\rangle, \quad (36)$$

where \hat{c}_H^\dagger creates a horizontally polarized photon, \hat{c}_V^\dagger creates a vertically polarized photon, and $|0\rangle$ is again the vacuum state.

Following the PBS, we let the creation operator \hat{c}^\dagger describe pump photons that travel clockwise about the Sagnac-like interferometer and we let \hat{d}^\dagger describe pump photons that travel counterclockwise. This gives the state of the pump after the PBS as

$$|\psi_{\text{pump}}\rangle = e^{-|\gamma_0|^2/2} e^{\gamma_0(\hat{c}_H^\dagger + \hat{d}_V^\dagger)/\sqrt{2}} |0\rangle, \quad (37)$$

where we have assumed that the PBS sends horizontally polarized photons clockwise about the Sagnac interferometer and vertically polarized photons counterclockwise.

Since we now have photons interacting with the PPKTP crystal from two different directions, we revise the Hamiltonian of Eq. (2) to now be

$$\hat{H} = i\kappa(\hat{c}_H^\dagger \hat{a}_H \hat{a}_V - \hat{c}_H \hat{a}_H^\dagger \hat{a}_V^\dagger) + i\kappa(\hat{d}_V^\dagger \hat{b}_H \hat{b}_V - \hat{d}_V \hat{b}_H^\dagger \hat{b}_V^\dagger), \quad (38)$$

where the \hat{a}^\dagger creation operators describe signal and idler photons traveling clockwise and the \hat{b}^\dagger creation operators describe signal and idler photons traveling counterclockwise.

Using the state of Eq. (37), we may now make the strong pump approximation by letting

$$\begin{aligned} \hat{c}_H &\rightarrow \langle \hat{c}_H \rangle = \frac{\gamma_0}{\sqrt{2}}, & \hat{c}_H^\dagger &\rightarrow \langle \hat{c}_H^\dagger \rangle = \frac{\gamma_0^*}{\sqrt{2}}, \\ \hat{d}_V &\rightarrow \langle \hat{d}_V \rangle = \frac{\gamma_0}{\sqrt{2}}, & \hat{d}_V^\dagger &\rightarrow \langle \hat{d}_V^\dagger \rangle = \frac{\gamma_0^*}{\sqrt{2}}, \end{aligned} \quad (39)$$

resulting in the approximate Hamiltonian

$$\hat{H} = i\frac{\kappa}{\sqrt{2}}(\gamma_0^* \hat{a}_H \hat{a}_V - \gamma_0 \hat{a}_H^\dagger \hat{a}_V^\dagger) + i\frac{\kappa}{\sqrt{2}}(\gamma_0^* \hat{b}_H \hat{b}_V - \gamma_0 \hat{b}_H^\dagger \hat{b}_V^\dagger). \quad (40)$$

If we let γ_0 be real and we redefine the squeezing parameter as $s \equiv \gamma_0 \kappa \tau / \sqrt{2}$, where τ is the interaction time inside the crystal, the unitary evolution operator for this method can now be represented as

$$\hat{U} = e^{s(\hat{a}_H \hat{a}_V - \hat{a}_H^\dagger \hat{a}_V^\dagger)} e^{s(\hat{b}_H \hat{b}_V - \hat{b}_H^\dagger \hat{b}_V^\dagger)}. \quad (41)$$

We can factor Eq. (41), just as was done in Eq. (5), giving

$$\hat{U} = \frac{e^{-\tanh(s)\hat{a}_H^\dagger\hat{a}_V^\dagger}}{\cosh^2(s)} \left[\frac{1}{\cosh(s)} \right]^{\hat{a}_H^\dagger\hat{a}_H + \hat{a}_V^\dagger\hat{a}_V} e^{\tanh(s)\hat{a}_H\hat{a}_V} \times e^{-\tanh(s)\hat{b}_H^\dagger\hat{b}_V^\dagger} \left[\frac{1}{\cosh(s)} \right]^{\hat{b}_H^\dagger\hat{b}_H + \hat{b}_V^\dagger\hat{b}_V} e^{\tanh(s)\hat{b}_H\hat{b}_V}. \quad (42)$$

Applying the operator of Eq. (42) to the vacuum state $|0\rangle$ and neglecting the pump gives the state after interaction with the PPKTP crystal as

$$|\psi\rangle = \frac{1}{\cosh^2(s)} e^{-\tanh(s)\hat{a}_H^\dagger\hat{a}_V^\dagger} e^{-\tanh(s)\hat{b}_H^\dagger\hat{b}_V^\dagger} |0\rangle. \quad (43)$$

We use the convention that when the different sets of photon pairs arrive at the PBS, the horizontal photons will be transmitted and the vertical photons will be reflected. We now let the transmitted path for the clockwise rotation be labeled path A and the counterclockwise rotation be path B. Therefore, the vertically polarized photons transform as

$$\hat{a}_V^\dagger \rightarrow \hat{b}_V^\dagger, \quad \hat{b}_V^\dagger \rightarrow -\hat{a}_V^\dagger. \quad (44)$$

Applying the transformation of Eq. (44) to the state given by Eq. (43) results in the state after the PBS $|\Psi_{\text{out}}\rangle$ being given by

$$|\Psi_{\text{out}}\rangle = \frac{1}{\cosh^2(s)} e^{-\tanh(s)\hat{a}_H^\dagger\hat{b}_V^\dagger} e^{\tanh(s)\hat{a}_V^\dagger\hat{b}_H^\dagger} |0\rangle = \sum_{j=0}^{\infty} \sum_{k=0}^{\infty} \frac{(-1)^j [\tanh(s)]^{j+k}}{j!k! \cosh^2(s)} \hat{a}_H^{\dagger j} \hat{a}_V^{\dagger k} \hat{b}_H^{\dagger k} \hat{b}_V^{\dagger j} |0\rangle. \quad (45)$$

Much like the state in Eq. (9) that was generated by the beam-splitter method of Fig. 1(a), the state in Eq. (45) does not resemble the ideal Bell state of Eq. (1). Again, letting $s \approx 0$ so that we only need to take terms up to $j = k = 1$ in Eq. (45) yields

$$\frac{1}{\cosh^2(s)} [1 - \tanh(s)(\hat{a}_H^\dagger\hat{b}_V^\dagger - \hat{a}_V^\dagger\hat{b}_H^\dagger)] |0\rangle. \quad (46)$$

Note that, unlike Eq. (11), the state of Eq. (46) does not contain terms where both photons enter the same path. This makes the entangled state generated from the Sagnac method of Fig. 1(b) more efficient than the beam-splitter method of Fig. 1(a). As we will see, this will be reflected in the resulting CHSH parameter for the situation when multiple pairs are generated.

B. Calculation of the CHSH parameter using the Husimi-Kano function

We now use the state of Eq. (45) to compute the CHSH parameter of Fig. 1(c). Applying the transformation of Eq. (12) to the state of Eq. (45) gives the state $|\psi\rangle$ after the polarization rotations of Fig. 1(c) as

$$|\psi\rangle = \frac{1}{\cosh^2(s)} e^{-\tanh(s)\cos(\theta_A - \theta_B)(\hat{a}_H^\dagger\hat{b}_V^\dagger - \hat{a}_V^\dagger\hat{b}_H^\dagger)} \times e^{-\tanh(s)\sin(\theta_A - \theta_B)(\hat{a}_H^\dagger\hat{b}_H^\dagger + \hat{a}_V^\dagger\hat{b}_V^\dagger)} |0\rangle. \quad (47)$$

Equation (47) appears simple; however, much like Eq. (13), we cannot simply use Eq. (47) in Eq. (15) to compute the co-

incidence rates. Therefore, we once again use the Q function to compute the coincidence rates of Eq. (15). The Q function for the state of Eq. (47) is given by

$$Q(\alpha_H, \alpha_V, \beta_H, \beta_V) = \frac{1}{\pi^4 \cosh^4(s)} e^{-(|\alpha_H|^2 + |\alpha_V|^2 + |\beta_H|^2 + |\beta_V|^2)} \times e^{-\tanh(s)\cos(\theta_A - \theta_B)(\alpha_H\beta_V + \alpha_H^*\beta_V^* - \alpha_V\beta_H - \alpha_V^*\beta_H^*)} \times e^{-\tanh(s)\sin(\theta_A - \theta_B)(\alpha_H\beta_H + \alpha_H^*\beta_H^* + \alpha_V\beta_V + \alpha_V^*\beta_V^*)}. \quad (48)$$

We now use the Q function of Eq. (48) in the rate integrals of Eq. (22). This distribution is also characterized by $N = 8$ and $\mu = \mathbf{0}$, so that we can read off the values of Σ^{-1} from Eq. (48), and subsequently invert Σ^{-1} to compute the covariance matrix Σ . The elements of Σ^{-1} in this case are given as

$$\begin{aligned} \Sigma_{11}^{-1} &= \Sigma_{22}^{-1} = \Sigma_{33}^{-1} = \Sigma_{44}^{-1} \\ &= \Sigma_{55}^{-1} = \Sigma_{66}^{-1} = \Sigma_{77}^{-1} = \Sigma_{88}^{-1} = 2, \\ \Sigma_{15}^{-1} &= -\Sigma_{26}^{-1} = \Sigma_{37}^{-1} = -\Sigma_{48}^{-1} \\ &= 2 \sin(\theta_A - \theta_B) \tanh(s), \\ \Sigma_{17}^{-1} &= -\Sigma_{28}^{-1} = -\Sigma_{35}^{-1} = \Sigma_{46}^{-1} \\ &= 2 \cos(\theta_A - \theta_B) \tanh(s), \end{aligned} \quad (49)$$

where, again, $\Sigma_{jk}^{-1} = \Sigma_{kj}^{-1}$ and the elements not listed are zero. Note that there are fewer nonzero elements in Eq. (49) than in Eq. (30). This is obvious from the fact that there are fewer terms in the exponent of Eq. (48) than in Eq. (20). Inverting Σ^{-1} gives the nonzero elements of the symmetric covariance matrix Σ as

$$\begin{aligned} \Sigma_{11} &= \Sigma_{22} = \Sigma_{33} = \Sigma_{44} = \Sigma_{55} \\ &= \Sigma_{66} = \Sigma_{77} = \Sigma_{88} = \frac{1}{2} \cosh^2(s), \\ -\Sigma_{15} &= \Sigma_{26} = -\Sigma_{37} = \Sigma_{48} \\ &= \frac{1}{4} \sin(\theta_A - \theta_B) \sinh(2s), \\ -\Sigma_{17} &= \Sigma_{28} = \Sigma_{35} = -\Sigma_{46} \\ &= \frac{1}{4} \cos(\theta_A - \theta_B) \sinh(2s). \end{aligned} \quad (50)$$

Using the elements of the covariance matrix in the expressions for the coincidence rates, such as Eq. (28), gives the coincidence rates for the Sagnac method as

$$\begin{aligned} R_{++} &= R_{--} = 1 + \cosh^4 s \\ &\quad - \cosh^2(s)[2 - \sinh^2(s)\sin^2(\theta_A - \theta_B)], \\ R_{+-} &= R_{-+} = 1 + \cosh^4 s \\ &\quad - \cosh^2(s)[2 - \sinh^2(s)\cos^2(\theta_A - \theta_B)]. \end{aligned} \quad (51)$$

Using these coincidence rates in the definition of the correlation coefficient of Eq. (14) gives

$$E(\theta_A, \theta_B) = -\frac{2 \cosh^2(s) \cos[2(\theta_A - \theta_B)]}{3 \cosh(2s) - 1}. \quad (52)$$

Finally, using the correlation coefficient of Eq. (52) in Eq. (16) gives the CHSH parameter as

$$|S| = 2\sqrt{2} \frac{2 \cosh^2(s)}{3 \cosh(2s) - 1}. \quad (53)$$

If we want to express Eq. (53) in terms of the mean number of pairs μ , we need to compute μ from Eq. (45). This is given as

$$\mu \equiv \langle (\hat{a}_H^\dagger \hat{a}_H + \hat{a}_V^\dagger \hat{a}_V)(\hat{b}_H^\dagger \hat{b}_H + \hat{b}_V^\dagger \hat{b}_V) \rangle = 2 \sinh^2(s). \quad (54)$$

Equation (54) now allows us to express Eq. (53) in terms of the mean number of photons, so that

$$|S| = 2\sqrt{2} \frac{2 + \mu}{2 + 3\mu}. \quad (55)$$

Equations (53) and (55) have been plotted in Fig. 2(b) using Eqs. (34) and (35). From Figs. 2(a) and 2(b), we see that the entanglement from the state generated by the beam-splitter method of Fig. 1(a) degrades as a function of the number of pairs more quickly than the entangled state generated by the Sagnac method of Fig. 1(b). This confirms that the Sagnac method of Fig. 1(b) is the more efficient method. Also, from Fig. 2(b), we see that the CHSH parameter initially decreases linearly as a function of μ , which represents a significant rate of reduction in the CHSH S parameter.

IV. CONCLUSION

In this article, we have introduced a rigorous theoretical model for the treatment of multiple photon pairs produced by SPDC sources. This model did not assume a maximum number of permitted photon pairs and potentially allows for infinite pairs. This was achieved using the Husimi-Kano Q function. This model shows that the CHSH parameter is dramatically reduced as the mean number of photon pairs μ increases above zero. This places serious limitations on the potential of SPDC sources to be used in robust quantum communication systems.

As was mentioned in the introduction, several other works have commented on this issue. Most of these works were either limited by a set number of additional pairs [29] or relied on a classical probability distribution [19,30–32]. The

classical distribution approach is capable of predicting the effect of multiple pairs in the Sagnac method of Fig. 1(b). Reference [19] computed the visibility of two-photon interference as a function of the mean number photons for the method of Fig. 1(b). This was computed using a Poissonian distribution and was compared to actual experimental data [19]. For small photon numbers, this model did not depend on the efficiency of the detection system and the resulting visibility was given as $V \approx 1 - \mu$ [19]. In our case, the two-photon interference visibility can be given as $V = |S|/2\sqrt{2}$ where S is defined in Eq. (55). If we let $\mu \approx 0$, then our visibility is also given by $V \approx 1 - \mu$, which agrees exactly with the result of Ref. [19]. The discrepancy for larger values of μ is likely due to the fact that Ref. [19] considered an inefficient detection system whereas we considered an ideal detection system for simplicity and to highlight the effects of multiple pairs. Additionally, Refs. [31,32] computed the two-photon interference visibility using a thermal distribution. The result for indistinguishable photons in Ref. [31] agrees exactly with our full $V = |S|/2\sqrt{2}$, where $|S|$ is given by Eq. (55).

While a classical probability distribution is capable of predicting the resulting CHSH parameter for the method shown in Fig. 1(b), it is unclear how a classical probability distribution could be used to give the result for the setup of Fig. 1(a). This is due to the additional quantum evolution given by the 50:50 beam splitter. This situation was easily computed through use of the Q function. We hope to use this method to compute the results of other, more complicated setups, as well as analyzing the impact of multiple photon pairs on teleportation [1] and entanglement swapping [39].

Multiple photon pairs are a critical issue for polarization-entangled states generated using the SPDC process. Understanding this issue is important for its mitigation and diagnosing experimental challenges. We have furthered this cause by establishing an all-quantum rigorous theoretical model rooted in a first-principles based approach.

ACKNOWLEDGMENTS

The authors acknowledge financial support from the U.S. Department of Defense (DOD) Contract No. H98230-19-D-0003/0017. They also acknowledge useful discussions with M. Morris and J. Goldhar.

-
- [1] C. H. Bennet, G. Brassard, C. Crépeau, R. Jozsa, A. Peres, and W. K. Wootters, Teleporting an Unknown Quantum State Via Dual Classical and Einstein-Podolsky-Rosen Channels, *Phys. Rev. Lett.* **70**, 1895 (1993).
 - [2] A. K. Ekert, Quantum Cryptography Based on Bell's Theorem, *Phys. Rev. Lett.* **67**, 661 (1991).
 - [3] J. D. Franson, Bell Inequality for Position and Time, *Phys. Rev. Lett.* **62**, 2205 (1989).
 - [4] C. K. Hong, Z. Y. Ou, and L. Mandel, Measurement of Subpicosecond Time Intervals Between Two Photons by Interference, *Phys. Rev. Lett.* **59**, 2044 (1987).
 - [5] C. Reimer, M. Kues, P. Roztockı, B. Wetzels, F. Grazioso, B. E. Little, S. T. Chu, T. Johnston, Y. Bromberg, L. Caspani, D. J. Moss, and R. Morandotti, Generation of multiphoton entangled quantum states by means of integrated frequency combs, *Science* **351**, 1176 (2016).
 - [6] A. Mair, A. Vaziri, G. Weihs, and A. Zeilinger, Entanglement of the orbital angular momentum states of photons, *Nature (London)* **412**, 313 (2001).
 - [7] M. Kues, C. Reimer, P. Roztockı, L. R. Cortés, S. Sciara, B. Wetzels, Y. Zhang, A. Cino, S. T. Chu, B. E. Little, D. J. Moss, L. Caspani, J. Azaña, and R. Morandotti, On-chip generation of high-dimensional entangled quantum states and their coherent control, *Nature (London)* **546**, 622 (2017).
 - [8] Y. K. Chembo, Quantum dynamics of Kerr optical frequency combs below and above threshold: Spontaneous four-wave mixing, entanglement, and squeezed states of light, *Phys. Rev. A* **93**, 033820 (2016).

- [9] B. Galmes, K. Phan-Huy, L. Furfaro, Y. K. Chembo, and J.-M. Merolla, Nine-frequency-path quantum interferometry over 60 km of optical fiber, *Phys. Rev. A* **99**, 033805 (2019).
- [10] A. Aspect, P. Grangier, and G. Roger, Experimental Realization of Einstein-Podolsky-Rosen-Bohm *Gedankenexperiment*: A New Violation of Bell's Inequalities, *Phys. Rev. Lett.* **49**, 91 (1982).
- [11] P. G. Kwiat, K. Mattle, H. Weinfurter, A. Zeilinger, A. V. Sergienko, and Y. Shih, New High-Intensity Source of Polarization-Entangled Photon Pairs, *Phys. Rev. Lett.* **75**, 4337 (1995).
- [12] G. Weihs, T. Jennewein, C. Simon, H. Weinfurter, and A. Zeilinger, Violation of Bell's Inequality Under Strict Einstein Locality Conditions, *Phys. Rev. Lett.* **81**, 5039 (1998).
- [13] D. S. Naik, C. G. Peterson, A. G. White, A. J. Berglund, and P. G. Kwiat, Entangled State Quantum Cryptography: Eavesdropping on the Ekert Protocol, *Phys. Rev. Lett.* **84**, 4733 (2000).
- [14] M. Li, C.-L. Zou, X.-F. Ren, X. Xiong, Y.-J. Cai, G.-P. Guo, L.-M. Tong, and G.-C. Guo, Transmission of photonic quantum polarization entanglement in a nanoscale hybrid plasmonic waveguide, *Nano Lett.* **15**, 2380 (2015).
- [15] C. E. Kuklewicz, M. Fiorentino, G. Messin, F. N. C. Wong, and J. H. Shapiro, High-flux source of polarization-entangled photons from a periodically poled KTiOPO₄ parametric down-converter, *Phys. Rev. A* **69**, 013807 (2004).
- [16] F. Kaiser, A. Issautier, L. A. Ngah, O. Alibert, A. Martin, and S. Tanzilli, A versatile source of polarization entangled photons for quantum network applications, *Laser Phys. Lett.* **10**, 045202 (2013).
- [17] T. Kim, M. Fiorentino, and F. N. C. Wong, Phase-stable source of polarization-entangled photons using a polarization Sagnac interferometer, *Phys. Rev. A* **73**, 012316 (2006).
- [18] C. Liang, K. F. Lee, M. Medic, P. Kumar, R. H. Hadfield, and S. W. Nam, Characterization of fiber-generated entangled photon pairs with superconducting single-photon detectors, *Opt. Express* **15**, 1322 (2007).
- [19] O. Kuzucu and F. N. C. Wong, Pulsed Sagnac source of narrow-band polarization-entangled photons, *Phys. Rev. A* **77**, 032314 (2008).
- [20] P. J. Thomas, C. J. Chunnillal, D. J. M. Stothard, D. A. Walsh, and M. H. Dunn, Production of degenerate polarization entangled photon pairs in the telecom-band from a pump enhanced parametric downconversion process, *Opt. Express* **18**, 26600 (2010).
- [21] E. Ji, Q. Liu, X. Fu, P. Du, M. Nie, F. Zhang, and M. Gong, High-brightness semiconductor laser-pumped 1.56 μm polarization-entangled photon pairs, *IEEE J. Quantum Electron.* **53**, 9300206 (2017).
- [22] H. Takesue and K. Inoue, Generation of Polarization-Entangled Photon Pairs and Violation of Bell's Inequality using Spontaneous Four-Wave Mixing in a Fiber Loop, *Phys. Rev. A* **70**, 031802(R) (2004).
- [23] X. Li, P. L. Voss, J. E. Sharping, and P. Kumar, Optical-Fiber Source of Polarization-Entangled Photons in the 1550-nm Telecom Band, *Phys. Rev. Lett.* **94**, 053601 (2005).
- [24] J. Fan, M. D. Eisaman, and A. Migdall, Bright phase-stable broadband fiber-based source of polarization-entangled photon pairs, *Phys. Rev. A* **76**, 043836 (2007).
- [25] Y.-H. Li, Z.-Y. Zhou, Z.-H. Xu, L.-X. Xu, B.-S. Shi, and G.-C. Guo, Multiplexed entangled photon-pair sources for all-fiber quantum networks, *Phys. Rev. A* **94**, 043810 (2016).
- [26] N. Akopian, N. H. Lindner, E. Poem, Y. Berlatzky, J. Avron, D. Gershoni, B. D. Gerardot, and P. M. Petroff, Entangled Photon Pairs from Semiconductor Quantum Dots, *Phys. Rev. Lett.* **96**, 130501 (2006).
- [27] J. F. Clauser, M. A. Horne, A. Shimony, and R. A. Holt, Proposed Experiment to Test Local Hidden-Variable Theories, *Phys. Rev. Lett.* **23**, 880 (1969).
- [28] B. S. Cirel'son, Quantum generalizations of Bell's inequality, *Lett. Math. Phys.* **4**, 93 (1980).
- [29] H. de Riedmatten, I. Marcikic, W. Tittel, H. Zbinden, and N. Gisin, Quantum interference with photon pairs created in spatially separated sources, *Phys. Rev. A* **67**, 022301 (2003).
- [30] H. Takesue and K. Inoue, 1.5- μm band quantum-correlated photon pair generation in dispersion-shifted fiber: Suppression of noise photons by cooling fiber, *Opt. Exp.* **13**, 7832 (2005).
- [31] H. Takesue and K. Shimizu, Effects of multiple pairs on visibility measurements of entangled photons generated by spontaneous parametric processes, *Opt. Commun.* **283**, 276 (2010).
- [32] H. S. Eisenberg, G. Khoury, G. A. Durkin, C. Simon, and D. Bouwmeester, Quantum Entanglement of a Large Number of Photons, *Phys. Rev. Lett.* **93**, 193901 (2004).
- [33] C. C. Gerry and P. L. Knight, *Introductory Quantum Optics* (Cambridge University Press, Cambridge, UK, 2005).
- [34] B. L. Schumaker and C. M. Caves, New formalism for two-photon quantum optics. II. Mathematical foundation and compact notation, *Phys. Rev. A* **31**, 3093 (1985).
- [35] S. M. Barnett and P. M. Radmore, *Methods in Theoretical Quantum Optics* (Oxford University Press, New York, 1997).
- [36] K. Husimi, Some formal properties of the density matrix, *Proc. Physico-Math. Soc. Japan, 3rd Ser.* **22**, 264 (1940).
- [37] Y. Kano, A new phase-space distribution function in the statistical theory of the electromagnetic field, *J. Math. Phys.* **6**, 1913 (1965).
- [38] W. P. Schleich, *Quantum Optics in Phase Space* (Wiley, Berlin, 2001).
- [39] B. Yurke and D. Stoler, Bell's-inequality experiments using independent-particle sources, *Phys. Rev. A* **46**, 2229 (1992).